Article

FRET-Created Traffic Light Immunoassay Based on Polymer Dots for PSA Detection

Yong-Quan Yang, Yu-Chi Yang, Ming-Ho Liu, and Yang-Hsiang Chan

Anal. Chem., **Just Accepted Manuscript** • DOI: 10.1021/acs.analchem.9b04747 • Publication Date (Web): 09 Dec 2019

FRET-Created Traffic Light Immunoassay Based on Polymer Dots for PSA Detection

Yong-Quan Yang,[a] Yu-Chi Yang,[a] Ming-Ho Liu,[a] and Yang-Hsiang Chan*[abc]

[a]Department of Applied Chemistry, National Chiao Tung University, Hsinchu, Taiwan 30010

[b]Center for Emergent Functional Matter Science, National Chiao Tung University, Hsinchu 30010, Taiwan

[c]Department of Medicinal and Applied Chemistry, Kaohsiung Medical University, Kaohsiung, Taiwan 80708

ABSTRACT: There have been enormous efforts for developing next generations of fluorometric lateral flow immunochromatographic strip (ICTS) owing to the great advances in fluorescent materials in these years. Here we developed one type of fluorometric ICTS based on ultrabright semiconducting polymer dots (Pdots) in which the traffic light-like signals were created by energy transfer depending on the target concentration. This platform was successfully applied for qualitatively rapid screening and quantitatively precise analysis of prostate-specific antigen (PSA) in 10 min from merely one drop of the whole blood sample. This FRET-created traffic light ICTS possesses the excellent specificity and an outstanding detection sensitivity of 0.32 ng/mL for PSA. Moreover, we conducted proof-of-concept experiments to demonstrate its potential for multiplexed detection of cancer biomarkers at the same time in an individual test strip by taking advantage of the traffic light signals. To the best of our knowledge, it is the first model of traffic light-like immunoassay test strip based on Pdots with multiplexing ability. These results would pave a avenue for designing the next generation of point-of-care diagnostics.

INTRODUCTION

Point-of-care (POC) detection, one type of in vitro diagnostic test, can provide reliable and accurate testing results in a timely manner.[1-3] As compared to traditional clinical diagnosis in a hospital which usually requires sophisticated instruments and professional operators, POC testing only needs to follow the simple instructions to obtain the test results in seconds to hours. Besides, most POC kits require merely small sample volumes (e.g., 1 μL - 1 mL) of complex physiological media to determine the target analytes in the range of picomolar to millimolar concentrations. This easy-to-handle, user-friendly, and cost-effective diagnostic approach is very suitable for on-the-spot patient care or in-home self-monitoring.

Lateral-flow immunochromatographic assays or the immunochromatography test strip (ICTS), is one of the most prevalent type of POC, which was ever developed by Unipath's PERSONA™ to measure luteinizing hormone and estriol-3-glucuronide in urine.[4] Nowadays, ICTS has been widely employed in diverse aspects, including clinical diagnostics, environmental inspection, forensic investigation, food safety/drug residue inspection, and health supervision.[1-3, 5-12] Despite of the impressive and flourishing development of ICTS, there are still several unmet challenges that might hinder its widespread use. For example, most ICTS platforms only allow for qualitative or semiquantitative analysis. Additionally, the detection sensitivity of ICTS is only adequate as compared to the most commonly used labeled immunoassay techniques, enzyme-linked immunosorbent assay (ELISA). Recently, enormous efforts have been exerted on promoting detection sensitivity of ICTS by exploring new types of signal reporting reagents. In contrast to traditional ICTS to utilize colloidal Au nanoparticles[2] as the signal reporter for colorimetric analysis in which the subtle variations of target concentrations are very difficult to be differentiated from the shades of Au nanoparticles. This limits their detection sensitivity as well as the quantitative ability. Fluorometric ICTS can cleverly circumvent the low sensitivity and quantitative concern of conventional colorimetric ICTS by employing fluorophores[5, 13-19] (e.g., small organic dyes, Au nanoclusters, up-converting nanoparticles, and quantum dots) as reporters. Among these fluorescent probes, inorganic quantum nanocrystals are the most extensively used one because of their exceptional photophysical properties.[20-22] However, quantum dots suffer from several issues like detrimental toxicity and active interactions with metal ions/biothiols in body fluids.[23-26] Therefore, exploitation of an ideal signal reporter remains an open challenge for fluorometric ICTS.

In our previous works,[27-28] we have successfully utilized highly bright semiconducting polymer nanoparticles (Pdots) as the fluorescent reporter in fluorometric ICTS for quantitative sensing of tumor antigens with sensitivity of about 100 times better than traditional colorimetric ICTS. The excellent performance of Pdot-based ICTS is attributed to the advantageous properties of Pdots:[29-49] (i) exceptional fluorescence brightness (over three orders of magnitude brighter than small organic molecules and quantum nanocrystals), offering high signal-to-noise ratios with minimal background signal; (ii) high colloidal stability in body fluids;[50-53] (iii) facile surface functionalization to conjugate with corresponding antibodies for specific immune detection; and (iv) amplified energy transfer in Pdots to enable the creation of multicolor emissions under single excitation wavelength, allowing for the design of multiplexed sensing systems with visual recognition functions.

In this work, we intended to design the first example of fluorescence resonance energy transfer (FRET)-based ICTS by exploiting the amplified energy in Pdots. Specifically, we would like to produce a change of the emission color on the test line depending on the concentration of the target analyte (prostatic specific antigen (PSA), a cancer biomarker of prostate cancer, in this study). The shift of the emission color on the test zone can be used for the prompt qualitative recognition and the quantitative analysis of PSA in whole-blood samples. As compared to traditional fluorometric ICTS with only one individual emission color, FRET-based ICTS with two or more emission colors embraces multiple unique advantages: (i) multiple emission colors can be used create a traffic light-like signal for rapid determination of the PSA levels by naked eyes; (ii) amplified energy transfer in Pdots results in the high FRET efficiency, allowing for the very sensitive determination of PSA concentration; and (iii) multiplexed detection capability benefited from the multicolor emissions. The innovative model of FRET-based ICTS could pave a new way in designing future generations of POC diagnostics.

EXPERIMENTAL SECTION

Chemicals. Deionized water (18.2 MΩ•cm) was applied in all of the experiments. Reaction reagents such as methanol, ethanol, hexane, ethyl acetate, acetone, piperidine, dichloromethane (CH_2Cl_2), 4,7,10-trioxa-1,13-tridecanediamine, *n*-hydroxysuccinimide (NHS), polyethylene glycol, octyl phenol ethoxylate, sodium hydroxide, poly(styrene-co-maleic anhydride), cumene terminated polymer with styrene of 75 wt. % (PSMA, M_n ~ 1900), tetrahydrofuran (THF), and *N*-(2-Hydroxyethyl)piperazine-*N*′-(2-ethanesulfonic acid) (HEPES) (CAS number 7365-45-9) were purchased from Sigma-Aldrich. Methoxypolyethylene glycol amine (PEG1000, M_w = 1000), tetrakis(triphenylphosphine)palladium(0), bovine serum albumin, saccharose, and 1-ethyl-3-(3-dimethylaminopropyl)carbodiimide (EDC) were obtained from Alfa Asear. PF-TC6FQ (M_n ~ 19 500) polymer was prepared based on our previously published works.[37] Carboxylic acid-functionalized polystyrenes (PS-PEG-COOH, product ID P18154-SEOCOOH, M_n = 18.0x10^3, M_w/M_n=1.09) was obtained from Polymer Source, Inc. PSA proteins (30C-CP1017U) and PSA primary antibodies (10-P20D and 10-P20E) were purchased from Fitzgerald (MA, USA). Mouse anti-human PSA primary antibodies were functionalized onto the surfaces of coumarin nanoparticles (10-P20E, capture antibody) and PF-TC6FQ Pdots (10-P20D, detection antibody), respectively. AffiniPure goat anti-mouse IgG (H+L) secondary antibodies (AB_2338447) were obtained from Jackson ImmunoResearch Inc. (PA, USA) and modified onto the control zone. These antibodies and antigens were diluted into the desired concentrations with HEPES buffer (pH 7.4) and then stably stored in the refrigerator for over 2 months. Nitrocellulose membranes (pore size = 15 μm, CNPC-SS12-L2-P25), sample pads (GFB-R7L), conjugate substrates (PT-R7), and absorbent matrices (AP 110) were got from Advanced Microdevices Pvt. Ltd.. The NC membranes, sample pads, conjugate pads, and absorbent pads were cut into 60 x 4 mm, 1.4 x 4 mm, 6 x 4 mm, and 2.1 x 4 mm (length x width), respectively. These above materials were finally assembled together and put inside the plastic cassettes. Green fluorescent coumarin derivatives, **CA**, was synthesized on the basis of the previously reported literatures with revised procedures.[54-56]

Synthesis of ethyl 7-(diethylamino)-2-oxo-2H-chromene-3-carboxylate, 1.[54] In a round glass flask was added 1.0 g (5.17 mmol) of 4-(diethylamino)-2-hydroxybenzaldehyde, 1.66 g (10.4 mmol) of diethyl malonate, and 0.2 mL (2.02 mmol) of piperidine in 6 mL of ethanol. The mixed solution was heated to 80 °C and refluxed for 8 h. After the reaction, the ethanol was removed by rotary evaporation and then the residue was added with CH_2Cl_2 to extract with water for three times. The CH_2Cl_2 layer was separated, dried by magnesium sulfate, and then the CH_2Cl_2 was evaporated by the rotary evaporator and vacuum system. The obtained yellow-brown oily compound was then purified using column chromatography on aluminum oxide, eluting by a mixture of CH_2Cl_2/ethyl acetate (10:1, v/v) solutions to get 997 mg (67 %) of compound **1** as yellow oil. ^{1}H NMR (400 MHz, $CDCl_3$): δ = 8.43 (s, 1H), 7.35 (d, J = 7.8 Hz, 1H), 6.60 (d, J = 7.8 Hz, 1H), 6.46 (s, 1H), 4.37 (q, J = 8.2 Hz, 2H), 3.44 (q, J = 3.8 Hz, 4H), 1.39 (t, J = 7.5 Hz, 3H), 1.23 (t, J = 7.3 Hz, 6H).

Synthesis of 7-(diethylamino)-2-oxo-2H-chromene-3-carboxylic acid, 2.[54] In a round flask into which 0.65 g (0.26 mmol) of compound **1** in 6 mL 0.5 M NaOH dissolved in methanol were added. The reaction was stirred at room temperature for 16 h and then neutralized with 4 mL of 1 M HCl. The mixture was kept at 4 °C for 24 h and the resulting precipitates were collected. The crude product was then purified via reprecipitation by using methanol/hexane to obtain 0.4 g (79 %) of compound **2** as an orange powder. ^{1}H NMR (400 MHz, $CDCl_3$): δ = 12.3 (s, 1H), 8.66 (s, 1H), 7.45 (d, J = 9.7 Hz, 1H), 6.71 (d, J = 6.0 Hz, 1H), 6.53 (s, 1H), 3.47 (q, J = 4.0 Hz, 4H), 1.26 (t, J = 7.5 Hz, 6H).

tert-butyl (3-(3-aminopropoxy)propyl)carbamate, 3.[55] 563 mg (2.56 mmol) of 4,7,10-trioxa-1,13-tridecanediamine was dissolved in 20 mL of dry CH_2Cl_2. For the other flask, 305 mg (1.40 mmol) of di-tert-butyl dicarbonate was dissolved in 20 mL of dry CH_2Cl_2. The solution containing di-tert-butyl dicarbonate was slowly added into the solution of 4,7,10-trioxa-1,13-tridecanediamine in an ice water bath. The reaction was further warmed to ambient temperature gradually and kept stirring for 16 h. The mixture was then extracted with brine for three times and the CH_2Cl_2 phase was isolated. After that, CH_2Cl_2 was removed by the rotary evaporator and vacuum system to yield 400 mg (49 %) of compound **3** as colorless oil. ^{1}H NMR (400 MHz, $CDCl_3$): δ = 3.64-3.52 (m, 12H), 3.21 (t, J = 6.4Hz, 2H), 2.80 (t, J = 6.7 Hz, 2H), 1.80-1.69 (m, 4H), 1.43 (s, 9H).

Synthesis of tert-butyl (3-(3-(7-(diethylamino)-2-oxo-2H-chromene-3-carboxamido)propoxy)propyl)carbamate, 4.[56] In a round glass flask where 384 mg (1.2 mmol) of compound **3**, 261 mg (1.00 mmol) of compound **2**, 288 mg (1.50 mmol) of EDC, and 173 mg (1.50 mmol) of NHS in 2 mL of CH_2Cl_2 were injected. The mixed solution was stirred at ambient temperature for 12 h. The organic phase was extracted with water for 3 times and isolated, dried by anhydrous $MgSO_4$. CH_2Cl_2 was further removed through rotary evaporation. The obtained product was then refined using column chromatography filled with Al_2O_3, eluting with CH_2Cl_2/ethyl

acetate (1:1, v/v) to afford 295 mg (35 %) of compound **4** as yellow oily liquid. ^{1}H NMR (400 MHz, $CDCl_3$): δ = 8.89 (s, 1H), 8.69 (s, 1H), 7.42 (d, J = 8.9 Hz, 1H), 6.64 (dd, J = 9.1, 2.6 Hz, 1H), 6.49 (s, 1H), 5.05 (s, 1H), 3.73-3.50 (m, 12H), 3.45 (q, J = 7.0 Hz, 4H), 3.22 (t, J = 7.6 Hz, 4H), 1.90 (d, J = 8.3 Hz, 2H), 1.75 (d, J = 8.3 Hz, 2H), 1.43 (s, 9H), 1.23 (t, J = 7.1 Hz, 6H).

Synthesis of N-(3-(3-aminopropoxy)propyl)-7-(diethylamino)-2-oxo-2H-chromene-3-carboxamide, CA.[56] 295 mg (0.52 mmol) of compound **4** was deprotected by trifluoroacetic acid (20%) in CH_2Cl_2 at room temperature for 12 h. The reaction was terminated by extracting with sodium bicarbonate aqueous solution (10%) for 3 times. The organic solvent was then removed to obtain 217 mg (90 %) of compound **CA** as brown liquid. ^{1}H NMR (400 MHz, $CDCl_3$): δ = 9.05 (s, 1H), 8.68 (s, 1H), 8.26 (s, 2H), 7.55 (d, J = 9.0 Hz, 1H), 6.71-6.63 (m, 1H), 6.49 (s, 1H), 3.83-3.50 (m, 12H), 3.46 (q, J = 7.4 Hz, 4H), 3.35-3.32 (m, 4H), 2.05 (d, J = 8.4 Hz, 2H), 1.85 (d, J = 8.4 Hz, 2H), 1.24 (t, J = 7.0 Hz, 6H).

Preparation of Polymer Nanoparticles. The preparation procedures of three Pdot stock THF solution were as follows: PF-TC6FQ, compound CA, and PSMA separately dissolved in THF with the concentration of 1000 ppm. 200 μL of PF-TC6FQ, 30 μL of PS-PEG-COOH, and 10 μL of PSMA were taken out and mixed well in 5 mL THF solution. The main purpose to use PS-PEG-COOH is to reduce the undesired biomolecule adsorption because of its polyethylene glycol units. PS-PEG-COOH can also provide the carboxylic units but the percentage of the grafted COOH group is lower than 10 % based on the manufacturer's analysis which might affect the efficiency of surface bioconjugation. Therefore, we added additional PSMA to offer the COOH terminal groups on the Pdot surface for further antibody conjugation. The THF mixture was then rapidly added to 10 mL of pure H_2O with intense sonication for ~ 30 s. THF was further evaporated by continuously blowing by N_2 gas on a 80 °C for 30-40 min. The as-prepared Pdot aqueous solution was kept purging with nitrogen gas at room temperature for 10 min and then passed through a 220 nm polyether sulfone syringe filter. For each batch, the final volume of the nanoparticle samples was tuned to ca. 8 mL and checked with UV-vis spectroscopy to ensure the fixed concentration of Pdots.

Preparation of coumarin (CA) nanoparticles. Compound CA was first conjugated with PSMA via EDC-catalyzed reactions. Specifically, 46.4 mg (0.1 mmol) of CA, 38 mg (0.02 mmol) of PSMA, 38 mg (0.2 mmol) of EDC, and 23 mg (0.2 mmol) of NHS were added into 2 mL of dichloromethane and then stirred for 30 min. After that, 20 mg (0.02 mmol) of PEG1000 was added and stirred for another 6 h. After the reaction, the mixture was extracted with water for three times and dichloromethane was removed by a rotary evaporator. The crude product was then purified by reprecipitation with dichloromethane/hexane to yield 50 mg of PSMA-grafted CA, compound PCA as an orange-yellow solid. For the preparation of CA nanoparticles, 200 μL of CA (1 mg/mL in THF) and 30 μL of PS-PEG-COOH were first mixed in 5 mL of THF. The CA-containing THF was further added to 10 mL of pure H_2O with intense sonication. THF was evaporated by continuously purging dry N_2 gas and then passed through a 220 nm polyether sulfone syringe filter.

Antibody Conjugation of PF-TC6FQ Pdots and CA Nanoparticles. For the bioconjugation of PF-TC6FQ Pdots, 2 mL of PF-TC6FQ, 40 μL of 1 M HEPES, 40 μL of 5% PEG (M_n = 3015-3685), 40 μL (1 mg/mL) of fresh-prepared EDC, 10 μL (1 mg/mL) of NHS, and 60 μL of PSA antibody (10-P20D, 0.1 mg/mL) were added in a vial and further reacted for 4 h at ambient temperature. Then, 2 μL (1 mg/mL) of PEG1000 was added and stirred for another 20 min. After the bioconjugation, the Pdot-PSA conjugates were refined by Sephacryl (S-300 HR) size exclusion chromatography resins to remove the free antibodies. The purified Pdot-PSA solution was further concentrated by a Pall Omega centrifugal device tube (molecular weight cut-off: 100 kDa) with the spinning setting of 1500 rpm for 5 min to get 400 μL of concentrated Pdot-PSA solution.

For CA-PSA bioconjugates that intended to be fabricated on the test line, 200 μL (1 mg/mL) of CA, 160 μL of 1M HEPES, 160 μL 5% PEG (M_n = 3015-3685), 6 μL (1 mg/mL) of fresh-prepared EDC, 1.5 μL (1 mg/mL) of NHS, and 37.5 μL of PSA antibody (10-P20E, 0.1 mg/mL) were added in a 2 mL of glass vial and let stir for 3 h. After the reaction, the CA-PSA conjugates were purified and concentrated by a standard 17 x 100 mm conical-end centrifuge tube (Pall Macrosep® Advance Centrifugal Devices, molecular weight cut-off: 10 kDa) to obtain a final volume of 25 μL.

For CA-BSA bioconjugates that intended to be fabricated on the control line, 8.0 mL (1 mg/mL) of CA, 160 μL of 1M HEPES, 160 μL 5% PEG (M_n = 3015-3685), 320 μL (1 mg/mL) of fresh-prepared EDC, 80 μL (1 mg/mL) of NHS, and 160 μL of bovine serum albumin (BSA) antibody (10 mg/mL) were added in a 20 mL of glass vial and let stir for 4 h. After the reaction, the CA-BSA conjugates were purified and concentrated by a standard 17 x 100 mm conical-end centrifuge tube (Pall Macrosep® Advance Centrifugal Devices, molecular weight cut-off: 10 kDa) to obtain a final volume of 400 μL with 10% glycerin.

Fabrication of Immunochromatography Test Strips for PSA Detection. The components of ICTS were modified in an effort to minimize the nonspecific interference. For nitrocellulose membranes, 0.05 % of glycerin aqueous solution was used to soak the membranes for 1 h and then dried under vacuum. For the pre-modification of conjugate pads, 5 % of glycerin aqueous solution was used instead. To fabricate the conjugate pads with Pdot probes, we first prepared a solution containing 20 μL of PF-TC6FQ Pdots, 15 μL of 20% sucrose, 5 μL of 20 mM HEPES buffer, and 40 μL of 5% glycerin; and then dipped the conjugate pads into the solution for 20 min. The modified conjugate pads were then dried under vacuum for 10 min. For the preparation of test samples, 0-30 μL of PSA (0.1 ng/μL), 32 μL of 10% PEG, 48 μL of 20 mM HEPES, and 10 % of human serum were mixed together for measurements. Human serum was used to mimic the physiological conditions of real samples and simultaneously could greatly reduce the undesired biomolecules binding. For the preparation of whole-blood analytes, we utilized a one-time-use sterile blood lancet to sting the fingertips to get one drop of fresh blood (5-10 μL) and then PSA proteins were added into the blood with the final concentrations of 1-12 ng/mL. The blood was dropped inside the sample port and then 80 μL of a buffer solution containing 32 μL of 10% PEG in 48 μL of 20 mM HEPES was added

inside the port promptly. While waiting for 10 min, the results could be recorded by a Nikon D7500 digital camera under the irradiation of 410 nm light irradiation with appropriate filters. For the blue and red emission, a band-pass filter of 470 ± 25 nm and a long-pass filter of 600 nm were used, respectively. The camera setting is: 1) F-stop: f/3.5; 2) Exposure time: 1/2-1/8 s; 3) ISO speed: ISO-500; 4) Exposure bias: -1 step; 5) Focal length: 18 mm; 6) Max aperture: 3.6; 7) Metering mode: Multi-zone; 8) Flash mode: No flash; 9) 35 mm focal length: 27; 10) Color temperature: 4000 K.

Characterization of FP/FG@Pdot Nanoparticles. The average sizes of PF-TC6FQ Pdots and PCA nanoparticles were measured using DLS instrument (Malvern Panalytical Zetasizer Nano Series). Transmission electron microscope images of PF-TC6FQ Pdots and PCA nanoparticles (diluted over 100 times) were obtained by a bio-transmission electron microscope (Hitachi, HT7700, accelerating voltage: 100-120 kV) The absorption spectra of Pdots and PCA nanoparticles were acquired by using a USB4000 miniature spectrometer (Ocean Optics, Inc.). Their corresponding emission spectra were measured by a Hitachi F-4500 fluorometer with an excitation wavelength at 400 nm. The fluorescence quantum yields of PF-TC6FQ Pdots and PCA nanoparticles were obtained using the integrating sphere detector in FS5-NIR fluorometer to be 0.40 and 0.27, respectively.

RESULTS AND DISCUSSION

Our aim was to utilize two types of Pdots with two distinct fluorescence colors (i.e., green and red fluorescence in this work) and then functionalized the corresponding antibodies onto the surface of Pdots. In the presence of target antigen, these two kinds of Pdots would anchor together on the test line of ICTS induced by the formation of the antibody-antigen sandwich complex. In this scenario, FRET would occur from the donor Pdots to the acceptor Pdots once the donor Pdots were excited, causing the combinations of two emission colors on the test line. The resulting emission color depends on the concentration of the target antigen. Ideally, we would like to create a traffic light-like signal based on FRET to mimic the low-medium-high concentrations of the target antigen. For example, the green emission represents the absence or low concentration of the target because there exists no FRET phenomenon. The intermediate color indicates the moderate concentration of the target antigen, while the red color implies the high concentration of the target antigen due to the obvious FRET behavior. This new FRET-based ICTS allows the direct qualitative visualization of the analyte from the emission color. Quantitative measurement of the analyte concentration could be further accomplished based on the relative intensities of green to red fluorescence.

Scheme 1. Synthetic Routes of Coumarin Derivatives

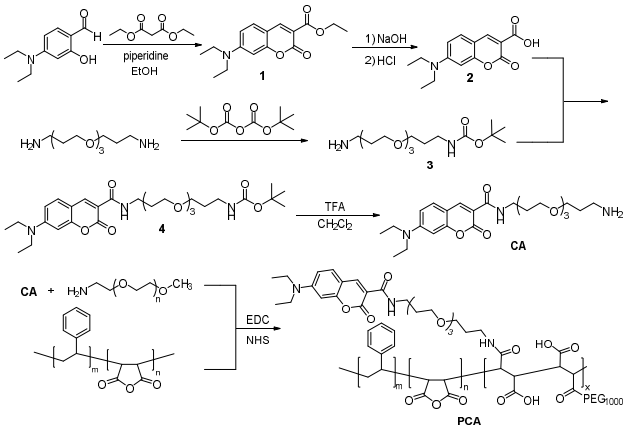

Selection and Optimization of Donor-Acceptor Pair. We wanted to create a FRET-based ICTS which can be excited by an individual source with two distinct fluorescent colors. The first aim was to select an appropriate donor-acceptor pair. Originally we purported to select green fluorescent Pdots, Poly[2,7-(9,9-dioctylfluorene)-alt-2,3-diphenylacrylonitrile] (PFCN), as the donor and paired them with red fluorescent Pdots, PF-TC6FQ, as the acceptor due to the substantial spectral overlap between the emission spectrum of PFCN and the absorption profile of PF-TC6FQ.[28] However, we found that PFCN Pdots could not be anchored onto the test line probably due to their hydrophilic surface properties and lack of anchoring groups on their surfaces. To tackle this issue, we synthesized a blue-green fluorescent coumarin derivative (CA) with an amine terminal group on the side chain as shown in Scheme 1. The coumarin dye 1 was first synthesized with an ethyl ester terminal moiety. The ethyl ester group was then hydrolyzed by sodium hydroxide to afford the carboxyl functional coumarin derivative 2. The compound 2 was reacted with compound 2 through EDC-catalyzed coupling to form compound 4. Finally, the tert-butoxycarbonyl group on compound 4 was deprotected by trifluoroacetic acid to obtain amine functional coumarin CA. We then conjugated compound CA and methoxypolyethylene glycol amine (PEG1000) with poly(styrene-co-maleic anhydride), cumene terminated polymer with styrene (PSMA) via EDC-catalyzed coupling. Here PSMA served as the polymer matrix to bind with green-emitting CA, while PEG1000 was used to reduce the non-specific adsorption. The ratio of CA to PEG1000 was optimized in an effort to maximize the fluorescence brightness and at the same time maintained the hydrophobic property of the resulting polymers, PCA.

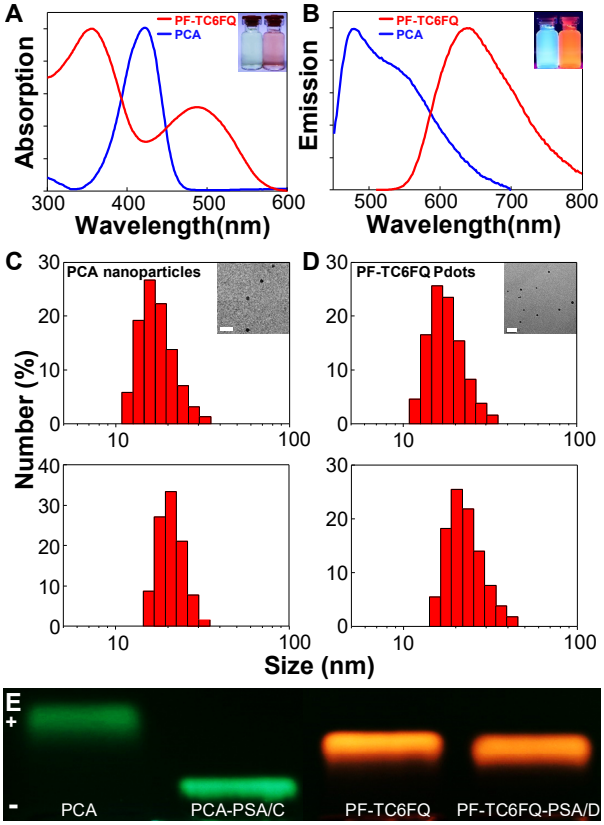

Figure 1. (A) Absorption spectra of PCA nanoparticles (blue line) and PF-TC6FQ Pdots (red line) in 20 mM HEPES buffer. The

Scheme 2. Schematic Diagram Illustrating the Design of FRET-Created Traffic Light ICTS[a]

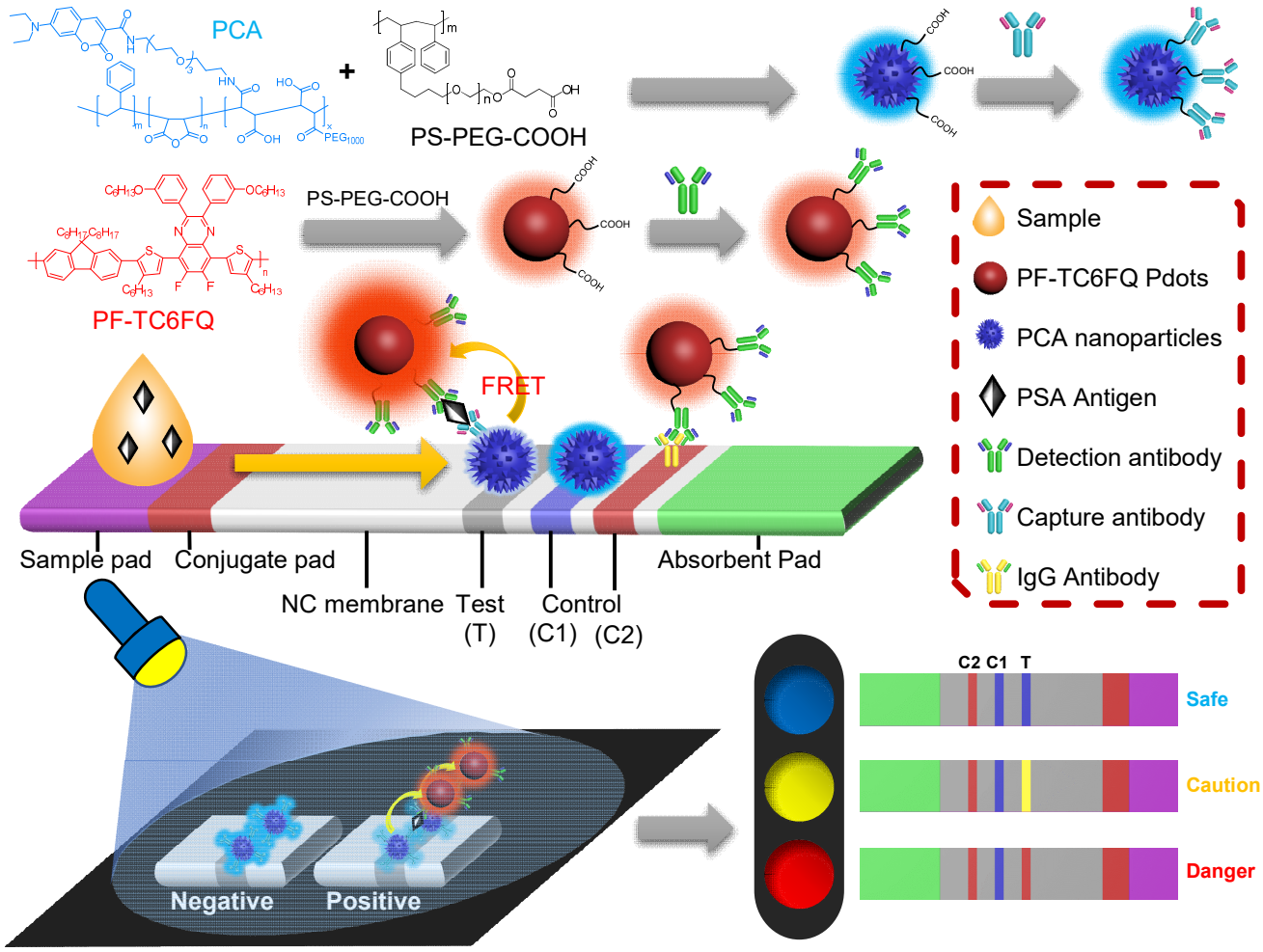

[a]First, coumarin derivative polymer (PCA) and semiconducting polymer (PF-TC6FQ) were synthesized and then mixed well in THF with carboxylic acid terminal polystyrene (PS-PEG-COOH) separately. PCA nanoparticles and PF-TC6FQ Pdots were prepared via nanoprecipitation by rapidly spiking the polymer THF mixtures into pure H_2O with intense sonication. PCA nanoparticles were further conjugated with PSA capture antibodies while PF-TC6FQ Pdots were conjugated with PSA detection antibodies. The PSA-modified PF-TC6FQ Pdots were fabricated onto the conjugate pad. There were two control lines on the nitrocellulose membrane: One was loaded with PCA nanoparticles and the other was decorated with IgG secondary antibodies. The test line was modified with PSA-modified PCA nanoparticles. This ICTS system allows the creation of traffic-light like signals based on FRET.

inset displays the photographic image of nanoparticle solutions in daylight (left: PCA nanoparticles; right: PF-TC6FQ Pdots). (B) Fluorescence spectra of PCA nanoparticles (blue line) and PF-TC6FQ Pdots (red line) in 20 mM HEPES buffer. The inset exhibits the photographic image of nanoparticle solutions excited by a UV lamp (left: PCA; right: PF-TC6FQ). (C) Hydrodynamic size distribution of PCA nanoparticles before (upper panel) and after (bottom panel) PSA capture antibody conjugation. The inset in the upper row represents the transmission electron microscopy image of as-prepared PCA nanoparticles. The scale bars are 100 nm. (D) Hydrodynamic size distribution of PF-TC6FQ Pdots before (upper panel) and after (bottom panel) PSA detection antibody conjugation. The inset in the upper row represents the transmission electron microscopy image of as-prepared PF-TC6FQ Pdots. (E) Gel electrophoresis of bare PCA/PF-TC6FQ nanoparticles and PSA-modified PCA/PF-TC6FQ nanoparticles. PSA/C and PSA/D: Capture and detection antibodies.

Surface Conjugation of PCA and PF-TC6FQ with Antibodies. Once we identified the possible donor-acceptor pair, we tested the FRET-based test strip for PSA detection. As displayed in Scheme 2, the modified PSMA polymers, PCA, were then co-precipitated with PS-PEG-COOH to genereate COOH functionalized PCA-based polymer nanoparticles. The PCA polymer nanoparticles were further conjugated with capture antibodies for PSA antigen detection. PF-TC6FQ Pdots were also prepared by nano-precipitation and then conjugated with detection antibodies. The absorption and fluorescence spectra of PCA nanoparticles and PF-TC6FQ were displayed in Figure 1A and B. The broad emission peak of PCA nanoparticles ranges from 490 nm to 600 nm, which overlaps very well with the second absorption band of PF-TC6FQ Pdots. This excellent spectral overlap between the emission profile of the PCA and the absorption profile of the PF-TC6FQ indicates that the FRET efficiency should be high (vide infra). Based on the UV-visible spectra in Figure 1A, we

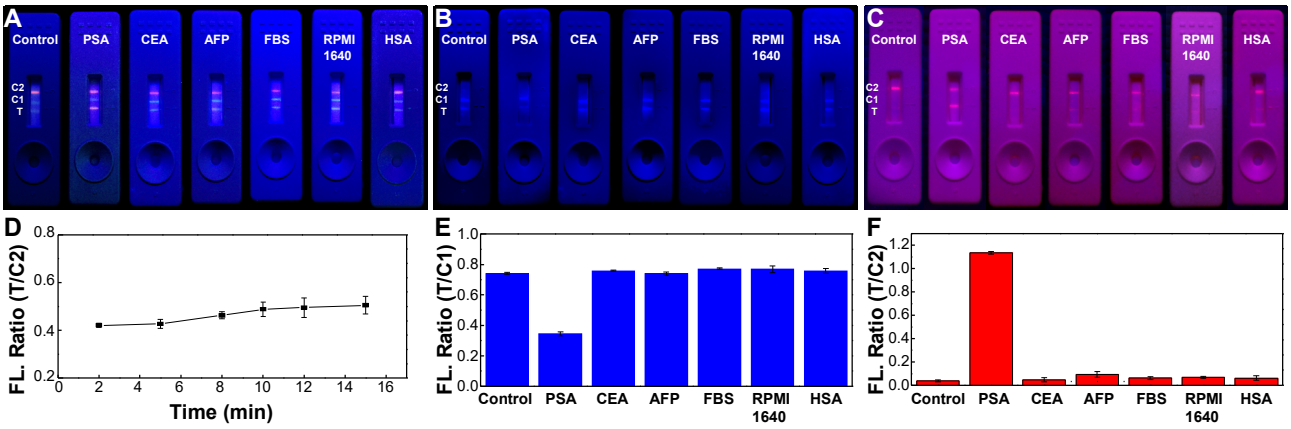

Figure 2. Assessment on the targeting specificity of the FRET-based immunochromatographic assays. Photographic images of the test strips after the detection of different analytes under 410 nm UV light (A) without filter, (B) with a band-pass filter of 470 ± 25 nm, and (C) with a long-pass filter of 600 nm. The concentrations of the antigens (PSA, CEA, and AFP), FBS, and human serum albumin (HSA) are 5 ng/mL, 5%, and 40 mg/mL, respectively. (D) Fluorescence ratios of the test zone to the second control zone at different times after the liquid reached the absorbent pad. (E) Quantitative emission ratios of T/C1 in panel B as determined by ImageJ software. (F) Quantitative emission ratios of T/C2 in panel C as calculated by ImageJ. The error bars in D-F show standard deviations obtained from over 5 replicates.

selected an excitation source of 410 nm to directly excite the PCA nanoparticles rather than the PF-TC6FQ Pdots. The average hydrodynamic size of the as-prepared PCA nanoparticles was determined by DLS to be 18 nm and increased to 23 nm after antibody conjugation as shown in Figure 1C. For PF-TC6FQ Pdots, the average diameter increased from 17 nm to 22 nm after antibody functionalization. The size increases could be attributed to the surface functionalization of PSA antibody (~29 kDa) as revealed in Figure 1D. We further executed gel electrophoresis to examine their surface charge properties and also measured their corresponding zeta potentials. The results in Figure 1E suggest that the antibody functionalization led to the slower electrophoretic mobility of the nanoparticles due to the reduction in the negative zeta potentials as well as the increased diameters of nanoparticles. The zeta potentials of PCA nanoparticles and PF-TC6FQ Pdots reduced from -34 mV to -26 mV and from -43mV to -28 mV, respectively. These results indicate the successful antibody conjugation on the nanoparticle/Pdot surfaces.

Detection Mechanism of FRET-Based ICTS. Once we successfully conjugated the PSA antibodies onto the surfaces of the nanoparticles, we can assemble these materials together in a lateral-flow test strip to evaluate their sensing performance. As depicted in Scheme 2, the conjugate pad was loaded with PSA (detection)-modified PF-TC6FQ Pdots. The microporous nitrocellulose membrane was fabricated with one test line (T) and two control lines (C1 and C2) for optimal comparison. For the test line, we tailored with PSA (capture)-functionalized PCA nanoparticles. For the control lines, the first one (C1) was made by bare PCA nanoparticles and the other one (C2) was modified with IgG secondary antibodies. Upon the addition of the blood samples onto the sample port, the blood cells were selectively blocked by the porous membrane and only the plasma/serum could migrate through the test strip via capillary flow. This means that this ICTS can be readily used for whole blood samples without pretreatment because the interferences such as red blood cells will be filtered out during migration. In the presence of PSA antigens, PF-TC6FQ Pdot-antibody conjugates were anchored on the test zone to form sandwich-shaped immune complexes. In this scenario, FRET occurred between the PCA nanoparticles and the PF-TC6FQ Pdots, generating the emission color transition from sky blue to orange red. As a result, the quenching of the PCA fluorescence and the enhancement of the PF-TC6FQ emission could be observed simultaneously. On the other hand, the absence of the PSA target biomarker led to a negative signal, in which no FRET occurred on the test line and thus the fluorescence of PCA nanoparticles remained unchanged. The first control was fabricated with bare PCA nanoparticles to serve as a reference of no FRET. The second control line was modified with IgG antibodies to selectively bind with PSA-functionalized PF-TC6FQ Pdots and then served as another reference of FRET. The detection results could be quickly interpreted by naked eyes under a portable 410 nm flashlight. More precise and quantitative analysis of the target concentration can be performed by measuring the emission ratios of the test line to the control line(s) (T/C1 or T/C2).

We first assessed the targeting specificity of these probes in ICTS. As shown in Figure 2A, the emission color on the test zone turned from blue sky to orange red after reaction with PSA proteins, indicating the occurrence of FRET phenomenon after the chelation of PCA with PF-TC6FQ. For the other samples, the emission of the test lines remained almost unchanged, suggesting negligible or minimal nonspecific protein adsorption and interference. Because the emission profile of PCA nanoparticles overlapped partially with that of PF-TC6FQ as shown in Figure 1B, we used filters to better observe the optical contrast. As displayed in Figure 2B, a band-pass filter of 470 ± 25 nm was employed to obtain the fluorescence from PCA nanoparticles alone. For the PSA sample, the fluorescence quenching of the test line could be seen as compared to that of the control line. The contrast, however, is not high enough for precise quantitative analysis due to the strong fluorescence background from the nitrocellulose membrane (Figure S1). On the contrary, the use of a long-pass filter of 600 nm produced a much higher contrast as shown in Figure 2C. These results indicate that the qualitative fast screening could be achieved by the emission color shift while the quantitative interpretation could be

realized based on fluorescence ratio of T/C2. The reaction time for this assay was set to 10 min because the T/C2 ratio reached a plateau at 10 min of running time (Figure 2D). It is worth mentioning that it took about 2 min for the sample to flow from sample pad to absorbent pad to have a detectable signal. The statistical analysis of the test strips (Figure 2E-F) again confirmed that the quantitative analysis could be performed based on emission ratios of T/C2.

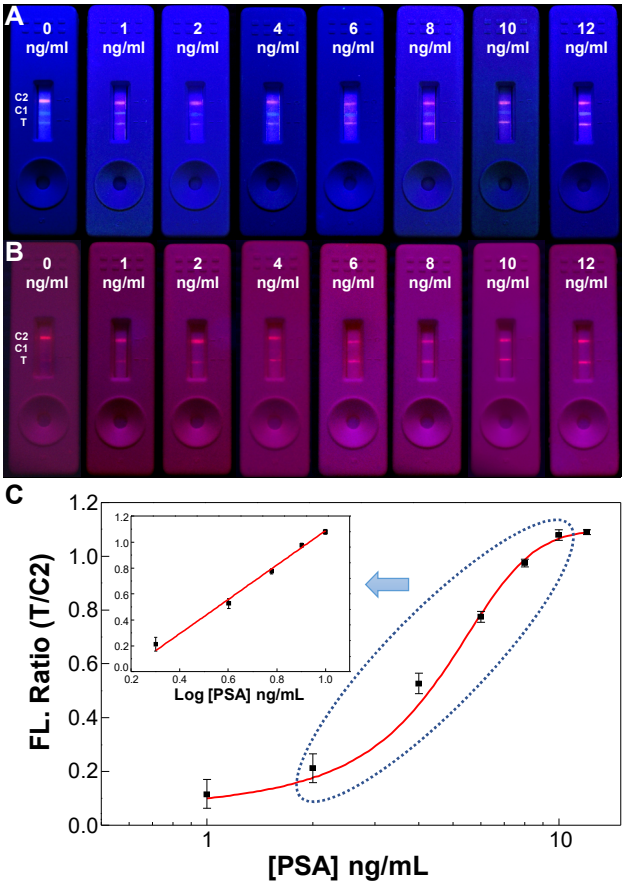

Figure 3. Quantitative analysis of PSA concentrations with FRET-based platforms. (A) Photographic images of ICTS under 410 nm UV excitation upon detection of analytes containing 0-12 ng/mL PSA antigens. (B) Their corresponding fluorescence photographs excited using a 410 nm lamp with a 600-nm long-pass filter. (C) The fluorescence intensity ratios of T/C2 with a long-pass filter of 600 nm. The upper-left corner inset exhibits the calibration curve with PSA concentrations ranging from 2 to 10 ng/mL. The error bars in C show standard deviations obtained from over 5 replicates.

Quantitative Analysis of PSA Biomarkers in Simulated Physiological Samples. The merit of the FRET-created traffic-light signals is that the emission color of the test line is directly relative to the target concentrations and can be easily recognized by the naked eye. The quantitative determination of the analyte concentrations could be further realized by measuring the emission intensity ratios of T/C. The simulated real samples we used here contain 0-30 μL of PSA (0.1 ng/μL), 32 μL of 10% PEG, 48 μL of 20 mM HEPES, and 10 % of human serum. The spiking of human serum helped simulate real analytes and could also reduce the nonspecific protein binding. The role of PEG is the same with human serum while it could at the same time prevent the sticking of Pdot probes onto the conjugate pad. From the images as exhibited in Figure 3A, it is obvious to find that the emission color of the test line turned from sky blue to intermediate yellow then red as the concentrations of PSA increased from 0 ng/mL to 12 ng/mL. The transition point fell between 4 ng/mL and 6 ng/mL, where the emission color transferred from yellow to red. This point is beneficial for rapid screening because PSA levels of over 4 ng/mL are recommended to proceed with a prostate biopsy for clear diagnosis of prostate cancer. The traffic-light signals were successfully realized by the FRET strategy in which the emission color on the test zone corresponded to the PSA level. The blue fluorescence on the test zone indicated a low PSA level (negligible FRET), while the appearance of yellow emission on the test line represented a middle PSA level (moderate FRET). The emergence of red emission on the test line, however, suggested a higher PSA level than the normal condition. This methodology highly enhanced the discriminability of the test results by directly recognizing the fluorescence color on the test line without the requirement of measuring its absolute fluorescence intensity like traditional ICTS. To further perform the quantitative analysis of PSA concentrations by this FRET-based ICTS, we used a 600-nm long-pass filter to selectively observe the fluorescence signal from PF-TC6FQ Pdots (Figure 3B) because the intensity of PF-TC6FQ is directly proportional to the concentration of PSA. The correlation between the emission intensities of T/C2 and PSA quantities was plotted in Figure 3C. A dynamic range from 2 to 10 ng/mL was displayed in the inset of Figure 3C. The limit of detection can be estimated by $3\sigma/m$,[28, 57-60] in which σ represents the standard deviation of the blank and m represents the slope of the calibration curve. The detection limit of PSA determined by this FRET-based ICTS platform is 0.32 ng/mL.

Table 1. Performance Evaluation of the FRET-Based Immunoassays in PSA-Spiked Blood.

analyte	[PSA] nominal (ng/mL)	[PSA] determined±SD (ng/mL)	Recovery (%)	CV (%)
PSA	2.00	2.05 ± 0.13	102	6.34
	4.00	3.82 ± 0.13	95	3.40
	6.00	5.85 ± 0.15	98	2.56
	8.00	7.96 ± 0.16	100	2.01
	10.00	9.77 ± 0.21	98	2.14

Measurement of PSA in Real Whole Blood Analytes. To further evaluate the practicality of this FRET-based ICTS in real human blood, we prepared fresh blood samples (from healthy volunteers) containing PSA by spiking known amount of PSA inside. The test results were summarized in Table 1 in which the number of the analytes is 5 for each concentration. The detection results exhibited the good agreement with the spiked values, indicating the high reliability of this platform. It is worth mentioning that the whole blood samples were directly used and the sample pretreatment was not required in this ICTS platform. This could highly eliminate the gross error in most ICTS systems. The test procedures were demonstrated in Video S1, where only one drop of blood was required for the test. The recovery values were all above 95% with CV of ca. 2-6 %. All of the aforementioned results suggest the facileness and potential of this FRET-based immunoassay for use in clinical analytes.

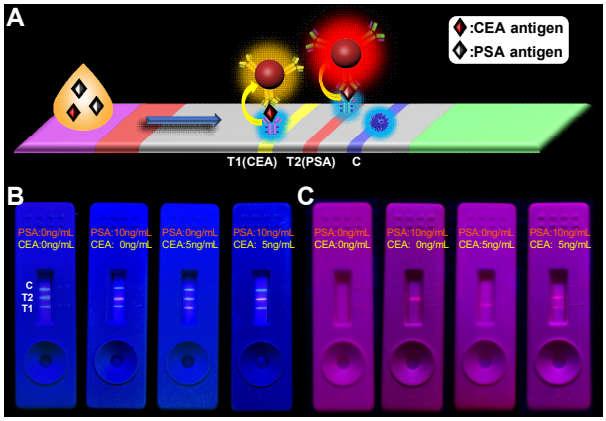

Figure 4. (A) Schematic illustrating the preparation of FRET-based ICTS with multiplexing sensing ability. (B) Photographic images of the test strips upon detection of analytes containing one or two tumor biomarker(s) under 410 nm light. (C) Their corresponding images with a long-pass filter of 600 nm.

Multiplexed Detection of PSA and CEA. One of the advantages of this FRET-based ICTS is its capability for detecting multiple targets in a single test strip. The fabrication of the test strips with multiplexing ability was illustrated in Figure 4A. In the test strip, we reserved only one control line made of bare PCA nanoparticles for color comparison. For the first test line (T1), we modified with carcinoembryonic antigen antibody (CEA, 10-7883)-functionalized PCA nanoparticles. The second test line was remined to be the PSA-functionalized PCA nanoparticles. Two conjugate pads consisting of PF-TC6FQ-CEA and PF-TC6FQ-PSA conjugates were stacked on top of each other. We first assess the specificity of this multiplexed ICTS, as exhibited in Figure 4B-C. It is obvious to find out that only the corresponding test line appeared to have FRET in the presence of the target antigen, indicating negligible cross reactivity of this test strip. We intentionally used a lower concentration of CEA (5 ng/mL) as compared to PSA (10 ng/mL) and were excited to found that the emission color discrepancy between two test lines could be distinguished (Figure 4B). With the aid of a long-pass filter, the fluorescence intensities from PF-TC6FQ Pdots could be easily quantified. This design is suitable for screening multiple targets simultaneously and provides the intuitive signals for health conditions. The above results demonstrated that the FRET-created traffic light ICTS has great potential for further development of POC systems in healthcare monitoring.

CONCLUSIONS

In summary, we developed a brand-new type of ICTS based on FRET-created signals for intuitive qualitative diagnosis and accurate quantitative detection of PSA biomarker. Each individual test requires only 1 drop (5-10 μL) of the whole blood sample without sample pretreatment and the test result can be interpreted in 10 min. Moreover, the limit of detection for the PSA antigen is about one order of magnitude lower than traditional fluorometric immunoassay systems. More importantly, multiplexed detection of tumor markers was successfully achieved by taking advantage of the high FRET efficiency. We anticipate this FRET-based methodology to have wide adoption in future generations of ICTS platforms.

ASSOCIATED CONTENT

Supporting Information.

This material is available free of charge via the Internet at DOI:
Supplementary data and NMR spectra.
Testing processes in whole blood analytes.

AUTHOR INFORMATION

Corresponding Author

*E-mail: yhchan@nctu.edu.tw

Notes

The authors declare no competing financial interest.

ACKNOWLEDGMENT

We would like to thank the MOST, Taiwan (grant No. 108-2113-M-009-023-MY3) and National Chiao Tung University for the research support.

REFERENCES

(1) Gubala, V.; Harris, L. F.; Ricco, A. J.; Tan, M. X.; Williams, D. E. Point of Care Diagnostics: Status and Future. *Anal. Chem.* **2012,** *84*, 487-515.
(2) Nayak, S.; Blumenfeld, N. R.; Laksanasopin, T.; Sia, S. K. Point-of-Care Diagnostics: Recent Developments in a Connected Age. *Anal. Chem.* **2017,** *89*, 102-123.
(3) Gauglitz, G. Point-of-Care Platforms. *Annu. Rev. Anal. Chem.* **2014,** *7*, 297-315.
(4) Wild, D. *The Immunoassay Handbook*, Third ed.; Elsevier: 2005.
(5) Li, X.; Li, W.; Yang, Q.; Gong, X.; Guo, W.; Dong, C.; Liu, J.; Xuan, L.; Chang, J. Rapid and Quantitative Detection of Prostate Specific Antigen with a Quantum Dot Nanobeads-Based Immunochromatography Test Strip. *ACS Appl. Mater. Interfaces* **2014,** *6*, 6406-6414.
(6) Song, C.; Liu, Q.; Zhi, A.; Yang, J.; Zhi, Y.; Li, Q.; Hu, X.; Deng, R.; Casas, J.; Tang, L.; Zhang, G. Development of a Lateral Flow Colloidal Gold Immunoassay Strip for the Rapid Detection of Olaquindox Residues. *J. Agric. Food Chem.* **2011,** *59*, 9319-9326.
(7) Li, Y.; Uddayasankar, U.; He, B.; Wang, P.; Qin, L. Fast, Sensitive, and Quantitative Point-of-Care Platform for the Assessment of Drugs of Abuse in Urine, Serum, and Whole Blood. *Anal. Chem.* **2017,** *89*, 8273-8281.
(8) Du, Y.; Pothukuchy, A.; Gollihar, J. D.; Nourani, A.; Li, B.; Ellington, A. D. Coupling Sensitive Nucleic Acid Amplification with Commercial Pregnancy Test Strips. *Angew. Chem. Int. Ed.* **2017,** *56*, 992-996.
(9) Song, J.; Mauk, M. G.; Hackett, B. A.; Cherry, S.; Bau, H. H.; Liu, C. Instrument-Free Point-of-Care Molecular Detection of Zika Virus. *Anal. Chem.* **2016,** *88*, 7289-7294.
(10) Zarei, M. Portable Biosensing Devices for Point-of-Care Diagnostics: Recent Developments and Applications. *Trends Anal. Chem.* **2017,** *91*, 26-41.
(11) Kumar, A. A.; Hennek, J. W.; Smith, B. S.; Kumar, S.; Beattie, P.; Jain, S.; Rolland, J. P.; Stossel, T. P.; Chunda-Liyoka, C.; Whitesides, G. M. From the Bench to the Field in Low-Cost Diagnostics: Two Case Studies. *Angew. Chem. Int. Ed.* **2015,** *54*, 5836-5853.
(12) Arts, R.; Hartog, I. d.; Zijlema, S. E.; Thijssen, V.; Beelen, S. H. E. v. d.; Merkx, M. Detection of Antibodies in Blood Plasma Using Bioluminescent Sensor Proteins and a Smartphone. *Anal. Chem.* **2016,** *88*, 4525-4532.
(13) Zhang, H.; Qiu, X.; Zou, Y.; Ye, Y.; Qi, C.; Zou, L.; Yang, X.; Yang, K.; Zhu, Y.; Yang, Y.; Zhou, Y.; Luo, Y. A Dye-Assisted Paper-Based Point-of-Care Assay for Fast and Reliable Blood Grouping. *Sci. Transl. Med.* **2017,** *9*, eaaf9209.
(14) Qiu, X.; Song, L.; Yang, S.; Guo, M.; Yuan, Q.; Ge, S.; Min, X.; Xia, N. A Fast and Low-Cost Genotyping Method for Hepatitis B virus Based on Pattern Recognition in Point-of-Care Settings. *Sci. Rep.* **2016,** *6*, 28274.

(15) Kim, Y.; Jang, G.; Lee, T. S. New Fluorescent Metal-Ion Detection Using a Paper-Based Sensor Strip Containing Tethered Rhodamine Carbon Nanodots. *ACS Appl. Mater. Interfaces* **2015,** *7*, 15649-15657.
(16) Zhao, Y.; Liu, X.; Wang, X.; Sun, C.; Wang, X.; Zhang, P.; Qiu, J.; Yang, R.; Zhou, L. Development and Evaluation of an Up-Converting Phosphor Technology-Based Lateral Flow Assay for Rapid and Quantitative Detection of Aflatoxin B1 in Crops. *Talanta* **2016,** *161* (297-303).
(17) Liu, X.; Zhao, Y.; Sun, C.; Wang, X.; Wang, X.; Zhang, P.; Qiu, J.; Yang, R.; Zhou, L. Rapid Detection of Abrin in Foods with an Up-Converting Phosphor Technology-Based Lateral Flow Assay. *Sci. Rep.* **2016,** *6*, 34926.
(18) Ren, M.; Xu, H.; Huang, X.; Kuang, M.; Xiong, Y.; Xu, H.; Xu, Y.; Chen, H.; Wang, A. Immunochromatographic Assay for Ultrasensitive Detection of Aflatoxin B1 in Maize by Highly Luminescent Quantum Dot Beads. *ACS Appl. Mater. Interfaces* **2014,** *6*, 14215-14222.
(19) Huang, X.; Aguilar, Z. P.; Li, H.; Lai, W.; Wei, H.; Xu, H.; Xiong, Y. Fluorescent Ru(phen)32+-Doped Silica Nanoparticles-Based ICTS Sensor for Quantitative Detection of Enrofloxacin Residues in Chicken Meat. *Anal. Chem.* **2013,** *85*, 5120-5128.
(20) Medintz, I. L.; Uyeda, H. T.; Goldman, E. R.; Mattoussi, H. Quantum Dot Bioconjugates for Imaging, Labelling and Sensing. *Nat. Mater.* **2005,** *4*, 435-446.
(21) Somers, R. C.; Bawendi, M. G.; Nocera, D. G. CdSe Nanocrystal Based Chem-/Bio-Sensors. *Chem. Soc. Rev.* **2007,** *36*, 579-591.
(22) Michalet, X.; Pinaud, F. F.; Bentolila, L. A.; Tsay, J. M.; Doose, S.; Li, J. J.; Sundaresan, G.; Wu, A. M.; Gambhir, S. S.; Weiss, S. Quantum Dots for Live Cells, in Vivo Imaging, and Diagnostics. *Science* **2005,** *307*, 538-544.
(23) Derfus, A. M.; Chan, W. C. W.; Bhatia, S. N. Probing the Cytotoxicity of Semiconductor Quantum Dots. *Nano Lett.* **2004,** *4*, 11-18.
(24) Brunetti, V.; Chibli, H.; Fiammengo, R.; Galeone, A.; Malvindi, M. A.; Vecchio, G.; Cingolani, R.; Nadeau, J. L.; Pompa, P. P. InP/ZnS as a Safer Alternative to CdSe/ZnS Core/Shell Quantum Dots: In Vitro and In Vivo Toxicity Assessment. *Nanoscale* **2013,** *5*, 307-317.
(25) Tsoi, K. M.; Dai, Q.; Alman, B. A.; Chan, W. C. W. Are Quantum Dots Toxic? Exploring the Discrepancy Between Cell Culture and Animal Studies. *Acc. Chem. Res.* **2013,** *46*, 662-671.
(26) Chan, Y.-H.; Chen, J.; Liu, Q.; Wark, S. E.; Son, D. H.; Batteas, J. D. Ultrasensitive Copper(II) Detection Using Plasmon-Enhanced and Photo-Brightened Luminescence of CdSe Quantum Dots. *Anal. Chem.* **2010,** *82*, 3671-3678.
(27) You, P.-Y.; Li, F.-C.; Liu, M.-H.; Chan, Y.-H. Colorimetric and Fluorescent Dual-Mode Immunoassay Based on Plasmon-Enhanced Fluorescence of Polymer Dots for Detection of PSA in Whole Blood. *ACS Appl. Mater. Interfaces* **2019,** *11*, 9841-9849.
(28) Fang, C.-C.; Chou, C.-C.; Yang, Y.-Q.; Wei-Kai, T.; Wang, Y.-T.; Chan, Y.-H. Multiplexed Detection of Tumor Markers with Multicolor Polymer Dot-Based Immunochromatography Test Strip. *Anal. Chem.* **2018,** *90*, 2134-2140.
(29) Pu, K.; Shuhendler, A. J.; Jokerst, J. V.; Mei, J.; Gambhir, S. S.; Bao, Z.; Rao, J. Semiconducting Polymer Nanoparticles as Photoacoustic Molecular Imaging Probes in Living Mice. *Nat. Nanotechnol.* **2014,** *9*, 233-239.
(30) Pu, K.; Chattopadhyay, N.; Rao, J. Recent Advances of Semiconducting Polymer Nanoparticles in In Vivo Molecular Imaging. *J. Control. Release* **2016,** *240*, 312.
(31) Lim, X. The Nanolight Revolution is Coming. *Nature* **2016,** *531*, 26-28.
(32) Wu, C.; Bull, B.; Szymanski, C.; Christensen, K.; McNeill, J. Multicolor Conjugated Polymer Dots for Biological Fluorescence Imaging. *ACS Nano* **2008,** *2*, 2415-2423.
(33) Wu, C.; Hansen, S. J.; Hou, Q.; Yu, J.; Zeigler, M.; Jin, Y.; Burnham, D. R.; McNeill, J. D.; Olson, J. M.; Chiu, D. T. Design of Highly Emissive Polymer Dot Bioconjugates for In Vivo Tumor Targeting. *Angew. Chem. Int. Ed.* **2011,** *50*, 3430-3434.
(34) Chan, Y.-H.; Wu, P.-J. Semiconducting Polymer Nanoparticles as Fluorescent Probes for Biological Imaging and Sensing. *Part. Part. Syst. Charact.* **2015,** *32*, 11-28.
(35) Li, S.; Wang, X.; Hu, R.; Chen, H.; Li, M.; Wang, J.; Wang, Y.; Liu, L.; Lv, F.; Liang, X.-J.; Wang, S. Near-Infrared (NIR)-Absorbing Conjugated Polymer Dots as Highly Effective Photothermal Materials for In Vivo Cancer Therapy. *Chem. Mater.* **2016,** *28*, 8669-8675.
(36) Lyu, Y.; Xie, C.; Chechetka, S. A.; Miyako, E.; Pu, K. Semiconducting Polymer Nanobioconjugates for Targeted Photothermal Activation of Neurons. *J. Am. Chem. Soc.* **2016,** *138*, 9049-9052.
(37) Liu, H.-Y.; Wu, P.-J.; Kuo, S.-Y.; Chen, C.-P.; Chang, E.-H.; Wu, C.-Y.; Chan, Y.-H. Quinoxaline-Based Polymer Dots with Ultrabright Red to Near-Infrared Fluorescence for In Vivo Biological Imaging. *J. Am. Chem. Soc.* **2015,** *137*, 10420-10429.
(38) Ke, C.-S.; Fang, C.-C.; Yan, J.-Y.; Tseng, P.-J.; Pyle, J. R.; Chen, C.-P.; Lin, S.-Y.; Chen, J.; Zhang, X.; Chan, Y.-H. Molecular Engineering and Design of Semiconducting Polymer Dots with Narrow-Band, Near-Infrared Emission for in Vivo Biological Imaging. *ACS Nano* **2017,** *11*, 3166-3177.
(39) Feng, L.; Zhu, C.; Yuan, H.; Liu, L.; Lv, F.; Wang, S. Conjugated Polymer Nanoparticles: Preparation, Properties, Functionalization and Biological Applications. *Chem. Soc. Rev.* **2013,** *42*, 6620-6633.
(40) Lyu, Y.; Zhen, X.; Miao, Y.; Pu, K. Reaction-Based Semiconducting Polymer Nanoprobes for Photoacoustic Imaging of Protein Sulfenic Acids. *ACS Nano* **2017,** *11*, 358-367.
(41) Lyu, Y.; Fang, Y.; Miao, Q.; Zhen, X.; Ding, D.; Pu, K. Intraparticle Molecular Orbital Engineering of Semiconducting Polymer Nanoparticles as Amplified Theranostics for in Vivo Photoacoustic Imaging and Photothermal Therapy. *ACS Nano* **2016,** *10*, 4472.
(42) Sun, K.; Tang, Y.; Li, Q.; Yin, S.; Qin, W.; Yu, J.; Chiu, D. T.; Liu, Y.; Yuan, Z.; Zhang, X.; Wu, C. In Vivo Dynamic Monitoring of Small Molecules with Implantable Polymer-Dot Transducer. *ACS Nano* **2016,** *10*, 6769-6781.
(43) Chen, X.; Li, R.; Liu, Z.; Sun, K.; Sun, Z.; Chen, D.; Xu, G.; Xi, P.; Wu, C.; Sun, Y. Small Photoblinking Semiconductor Polymer Dots for Fluorescence Nanoscopy. *Adv. Mater.* **2017,** *29*, 1604859.
(44) Tsai, W. K.; Chan, Y. H. Semiconducting Polymer Dots as Near-Infrared Fluorescent Probes for Bioimaging and Sensing. *J. Chin. Chem. Soc.* **2019,** *66*, 9-20.
(45) Jiang, Y.; Pu, K. Multimodal Biophotonics of Semiconducting Polymer Nanoparticles. *Acc. Chem. Res.* **2018,** *51*, 1840-1849.
(46) Zhen, X.; Xie, C.; Pu, K. Temperature-Correlated Afterglow of a Semiconducting Polymer Nanococktail for Imaging-Guided Photothermal Therapy. *Angew.Chem. Int. Ed.* **2018,** *57*, 3938-3942.
(47) Jiang, Y.; McNeill, J. Light-Harvesting and Amplified Energy Transfer in Conjugated Polymer Nanoparticles. *Chem. Rev.* **2017,** *117*, 838-859.
(48) Miao, Q.; Xie, C.; Zhen, X.; Lyu, Y.; Duan, H.; Liu, X.; Jokerst, J. V.; Pu, K. Molecular Afterglow Imaging with Bright, Biodegradable Polymer Nanoparticles. *Nat. Biotechnol.* **2017,** *35*, 1102-1110.
(49) Li, J.; Huang, J.; Lyu, Y.; Huang, J.; Jiang, Y.; Xie, C.; Pu, K. Photoactivatable Organic Semiconducting Pro-nanoenzymes. *J. Am. Chem. Soc.* **2019,** *141*, 4073-4079.
(50) Singh, A.; Bezuidenhout, M.; Walsh, N.; Beirne, J.; Felletti, R.; Wang, S.; Fitzgerald, K. T.; Gallagher, W. M.; Kiely, P.; Redmond, G. Functionalization of Emissive Conjugated Polymer Nanoparticles by Coprecipitation: Consequences for Particle Photophysics and Colloidal Properties. *Nanotechnol.* **2016,** *27*, 305603.
(51) Zhang, X.; Yu, J.; Wu, C.; Jin, Y.; Rong, Y.; Ye, F.; Chiu, D. T. Importance of Having Low-Density Functional Groups for Generating High-Performance Semiconducting Polymer Dots. *ACS Nano* **2012,** *6*, 5429-5439.
(52) Wei, L.; Zhang, D.; Zheng, X.; Zeng, X.; Zeng, Y.; Shi, X.; Su, X.; Xiao, L. Fabrication of Positively Charged Fluorescent Polymer Nanoparticles for Cell Imaging and Gene Delivery. *Nanotheranostics* **2018,** *2*, 157-167.

(53) Prakash, K. Passivation and Functionalization of Conjugated Polymer Nanoparticles with Head Group Modified Phospholipids and Proteins. *All Dissertations* **2014**, 1302.
(54) Ng, C. Y.; Kwok, T. X. W.; Tan, F. C. K.; Low, C.-M.; Lam, Y. Fluorogenic Probes to Monitor Cytosolic Phospholipase A_2 Activity. *Chem. Commun.* **2017,** *53*, 1813-1816.
(55) Liu, W.; Li, F.; Chen, X.; Hou, J.; Yi, L.; Wu, Y.-W. A Rapid and Fluorogenic TMP-AcBOPDIPY Probe for Covalent Labeling of Proteins in Live Cells. *J. Am. Chem. Soc.* **2014,** *136*, 4468-4471.
(56) Kunishima, M.; Kato, D.; Nakanishi, S.; Kitamura, M.; Yamada, K.; Terao, K.; Asano, T. Specific Labeling of Streptavidin for Better Understanding of Ligand Modification in Modular Method for Affinity Labeling (MoAL). *Chem. Pharm. Bull.* **2014,** *62*, 1146-1150.
(57) Zhu, D.; Xue, L.; Li, G.; Che, Y.; Jiang, H. A Turn-On Fluorescent Probe for Detection of Hydrogen Sulfide in Aqueous Solution and Living Cells. *Org. Chem. Front.* **2014,** *1*, 501-505.
(58) Alam, P.; Leung, N. L. C.; Su, H.; Qiu, Z.; Kwok, R. T. K.; Lam, J. W. Y.; Tang, B. Z. A Highly Sensitive Bimodal Detection of Amine Vapours Based on Aggregation Induced Emission of 1,2‐Dihydroquinoxaline Derivatives. *Chem. Eur. J.* **2017,** *23*, 14911-14917.
(59) Lima, F. M. d. R.; Freires, A. d. S.; Pereira, N. d. M.; Silva, G. G.; Rocha, C. Q. d.; Damos, F. S.; Luz, R. d. C. S. Photoelectrochemical Sensing of Tannic Acid Based on the Use of TiO_2 Sensitized with 5-Methylphenazinium Methosulfate and Carboxy-Functionalized CdTe Quantum Dots. *Microchimica Acta.* **2018,** *185*, 521.
(60) Pei, X.; Kang, W.; Yue, W.; Bange, A.; Heineman, W. R.; Papautsky, I. Disposable Copper-Based Electrochemical Sensor for Anodic Stripping Voltammetry. *Anal. Chem.* **2014,** *86*, 4893-4900.

For Table of Contents only